Capturing photons with transformation optics

Luo, Yu; Zhao, Rongkuo; Fernández-Domínguez, A.I.; Pendry, J.B.

2013

https://hdl.handle.net/10356/79352

https://doi.org/10.1038/nphys2667

Capturing Photons with Transformation Optics

J.B. Pendry[*], A.I. Fernández-Domínguez[*], Yu Luo[*], and Rongkuo Zhao[*]

The Blackett Laboratory, Department of Physics, Imperial College London, London SW7 2AZ, United Kingdom

Metallic objects in close contact and illuminated by light show spectacular enhancements of electromagnetic fields, due to excitation of surface plasmons, which have potential for exploitation in ultra sensitive spectroscopy and in nonlinear phenomena. They also play a role in Van der Waals forces, heat transfer, and non contact friction. The extremes of length scales, varying from the micron to the sub nano, challenge direct computational attack. Here we show that the new technique of transformation optics enables an analytic approach which offers both physical insight and easy access to quantitative analysis. For two metal spheres at various separations we present details of the new technique, discuss the optical absorption spectrum, spatial distribution of the modes, and the Van der Waals forces.

[*]These authors are deemed to have contributed equally.

Transformation optics is a powerful new tool, exact at the level of Maxwell's equations [1-3]. Reviews can be found in [4-6]. Amongst other applications it has been used to shape the design variants of the perfect lens [7,8] and design cloaks of invisibility [9,10]. Here we apply the technique to gain understanding of the optical interaction between two nanospheres.

To control light on the nanoscale has been the goal of much recent research. Central to these efforts have been the electron density oscillations at the surfaces of metals known as surface plasmons and in particular the geometrical structure of the surface that greatly influences their properties. Several authors have shown that structural singularities in the form of cusps or sharp points can capture incident radiation and concentrate its energy into nanometric volumes [11-19]: see [6,20] for a review. With recent experimental advances nanoscale geometry can be accurately defined and controlled, opening the door to practical exploitation of these effects but also demanding a detailed theoretical understanding. The new technique of transformation optics offers valuable physical insights into the singular phenomena. We have applied the technique extensively to 2D systems such as touching cylinders and sharp edges [6]. However that work described only the subset of the spectrum with electric fields perpendicular to the cylinder axis. Here we extend the reach to 3D systems and give a complete description of the spectra which enables us to reach beyond a description of the spectroscopy to other phenomena such as Van der Waals interactions. Specifically we study two spheres separated by an arbitrary distance, and classify the extraordinary character of that system's excitations. As well as yielding physical insight our methodology gives rise to an accurate and extremely efficient computational scheme which will be of value in further studies of this and related systems.

When two metal surfaces come close to touching their surface plasmons strongly hybridise [21]. This has consequences for mechanical forces between the surfaces, for heat transfer between the surfaces, and for frictional forces which come into play when the surfaces are in relative motion. Also the point of closest approach becomes a harvesting point for incident radiation which tends to be concentrated at the point of near contact. Two nearly touching spheres constitute a paradigm for a whole class of systems some of which can be directly related through transformation optics, and others such as two curved surfaces which can be approximated near their point of closest approach by two spheres.

Our goal is to find a near-analytic solution for the electromagnetic modes of two spheres in close proximity. We shall assume that the spheres are small and all dimensions less than free space optical wavelengths, enabling us to work in the quasi-static approximation. Radiative corrections can be applied as described in [6]. We also assume a local model for the permittivity but recognise that non locality and electron tunnelling are important at extremely small separations [22-25]. We leave investigation of these effects for a later paper. The standard transformation optics approach is to start from a system that is easy to solve, then transform the geometry to the desired system. Transformation optics tells how we must change the parameters of the system (the permittivity, ϵ, and permeability, μ) in order to have a valid solution of Maxwell's equations. Our starting system is shown in Fig. 1.

The annular system of Fig. 1a has much more symmetry than the system in Fig. 1b, and this will help with the solution. The two systems are related by a transformation defined by,

$$\mathbf{r}'-\mathbf{R}'_0 = R_T^2 \frac{\mathbf{r}-\mathbf{R}_0}{\left|\mathbf{r}-\mathbf{R}_0\right|^2}, \tag{1}$$

which maps points at infinity to the origin, points at the origin to infinity, and transforms a sphere into another sphere. R_T is a parameter of the transformation. Essentially the system is turned inside out. Another inversion about the new origin takes the system in Fig. 1b back to the original system shown in Fig. 1a.

$$\mathbf{r}-\mathbf{R}_0 = R_T^2 \frac{\mathbf{r}'-\mathbf{R}'_0}{\left|\mathbf{r}'-\mathbf{R}'_0\right|^2}. \tag{2}$$

Note that the region of closest approach in Fig. 1b maps into the region furthest from the origin in Fig. 1a.

We shall assume that the system in Fig. 1b comprises homogeneous metals defined by a permittivity ϵ'_M, immersed in a homogeneous dielectric defined by ϵ'_D. Since we work in the quasi-static approximation we shall ignore the permeability. Transformation optics guarantees that any potential, $\phi(\mathbf{r})$, that is a valid solution for the system in Fig. 1a is also valid for in Fig. 1b, $\phi(\mathbf{r}')$, provided that the permittivities in Fig. 1a satisfy,

$$\varepsilon^{ij} = \left[\det(\Lambda)\right]^{-1} \Lambda^i_{i'} \Lambda^j_{j'} \varepsilon'^{\,i'j'}, \tag{3}$$

where, $\Lambda^j_{j'} = \partial x^j / \partial x'^{j'}$.

For the inversion defined by (2) this works out to give,

$$e(\mathbf{r}) = R_T^2 |\mathbf{r} - \mathbf{R}_0|^{-2} e'(\mathbf{r}'). \tag{4}$$

In other words the system is no longer homogeneous. However this turns out to be a minor complication because it is well known that $j(\mathbf{r})$ can be written as $j(\mathbf{r}) = |\mathbf{r} - \mathbf{R}_0| V(\mathbf{r})$, where $V(\mathbf{r})$ is a solution of Laplace's equation, $\nabla^2 V(\mathbf{r}) = 0$.

Our strategy is to solve for $j(\mathbf{r})$ in the simplified geometry of the annulus and hence find $j(\mathbf{r}')$ and to this end we expand in spherical harmonics choosing as the origin the centre of the spheres,

$$\begin{aligned}
j &= a_{\ell m}^{in} |\mathbf{r} - \mathbf{R}_0| r^{\ell} Y_{\ell m}(\theta,\phi), \quad r < R_1, \\
j &= |\mathbf{r} - \mathbf{R}_0| \left[\left(a_{\ell m}^{+} + a_{\ell m}^{s+} \right) r^{\ell} + a_{\ell m}^{-} r^{-(\ell+1)} \right] \\
&\quad \times Y_{\ell m}(\theta,\phi), \qquad R_0 > r > R_1, \\
j &= |\mathbf{r} - \mathbf{R}_0| \left[a_{\ell m}^{+} r^{\ell} + \left(a_{\ell m}^{-} + a_{\ell m}^{s-} \right) r^{-(\ell+1)} \right] \\
&\quad \times Y_{\ell m}(\theta,\phi), \qquad R_2 > r > R_0, \\
j &= |\mathbf{r} - \mathbf{R}_0| a_{\ell m}^{out} r^{-(\ell+1)} Y_{\ell m}(\theta,\phi), \quad r > R_2.
\end{aligned} \tag{5}$$

Here $a_{\ell m}^{s\pm}$ are source terms feeding energy into the system.

We need to match the potential across both surfaces of the annulus, and also match $e\mathbf{r} \cdot \nabla j$. Although the azimuthal angular momentum, m, is conserved, the total angular momentum, ℓ, is not conserved because the factor $|\mathbf{r} - \mathbf{R}_0|$ spoils the spherical symmetry. However it does so in a rather gentle fashion coupling the equations only to $\ell \pm 1$ resulting in a tridiagonal system of equations which, although not in general analytically soluble, is easily solved numerically and in limiting cases analytically. The result is a matrix equation,

$$\begin{bmatrix} \mathbf{S}^{++} & \mathbf{0} \\ \mathbf{0} & \mathbf{S}^{--} \end{bmatrix} \begin{bmatrix} \mathbf{a}^{s+} \\ \mathbf{a}^{s-} \end{bmatrix} = \begin{bmatrix} \mathbf{T}^{++} & \mathbf{T}^{+-} \\ \mathbf{T}^{-+} & \mathbf{T}^{--} \end{bmatrix} \begin{bmatrix} \mathbf{a}^{+} \\ \mathbf{a}^{-} \end{bmatrix}, \tag{6}$$

in which each quadrant of the matrices is tridiagonal:

$$
\begin{aligned}
\tilde{S}^{++}_{\ell\ell'} &= +\delta_{\ell\ell'}\left[\ell'\left(r_1^2+1\right)+r_1^2\right] \\
&\quad -\left(2\ell'+1\right)\left(\delta_{\ell\ell'+1}A^{+}_{\ell}r_1^{-1}R_0^{-1}+\delta_{\ell\ell'-1}A^{-}_{\ell}r_1R_0\right)r_1, \\
\tilde{S}^{--}_{\ell\ell'} &= -\delta_{\ell\ell'}\left[\left(\ell'+1\right)\left(r_2^2+1\right)-r_2^2\right] \\
&\quad +\left(2\ell'+1\right)\left(\delta_{\ell\ell'+1}A^{+}_{\ell}r_2R_0+\delta_{\ell\ell'-1}A^{-}_{\ell}r_2^{-1}R_0^{-1}\right)r_2,
\end{aligned}
\tag{7}
$$

$$
\begin{aligned}
A^{+}_{\ell} &= \left[\frac{1}{\left(2\ell+1\right)\left(2\ell+3\right)}\right]^{\frac{1}{2}}\left[\left(\ell+1\right)^2-m^2\right]^{\frac{1}{2}}, \\
A^{-}_{\ell} &= \left[\frac{1}{\left(2\ell+1\right)\left(2\ell-1\right)}\right]^{\frac{1}{2}}\left[\ell^2-m^2\right]^{\frac{1}{2}},
\end{aligned}
\tag{8}
$$

$$
\begin{aligned}
\tilde{T}^{++}_{\ell\ell'} &= -\tilde{S}^{++}_{\ell\ell'}, \quad \tilde{T}^{--}_{\ell\ell'} = -\tilde{S}^{--}_{\ell\ell'}, \\
\tilde{T}^{+-}_{\ell\ell'} &= \left[+\delta_{\ell\ell'}\frac{r_1^2-1}{\left(\varepsilon'_M-1\right)}-\tilde{S}^{++}_{\ell\ell'}e^{-\alpha}\right]R_1^{-\left(2\ell'+1\right)}, \\
\tilde{T}^{-+}_{\ell\ell'} &= \left[+\delta_{\ell\ell'}\frac{r_2^2-1}{\left(\varepsilon'_M-1\right)}-\tilde{S}^{--}_{\ell\ell'}e^{-\alpha}\right]R_2^{+\left(2\ell'+1\right)},
\end{aligned}
\tag{9}
$$

where

$$
e^{\alpha}=\frac{\varepsilon'_M-\varepsilon'_D}{\varepsilon'_M+\varepsilon'_D} \tag{10}
$$

and $r_{1,2}=R_{1,2}/R_0$. Such matrices can be rapidly inverted and diagonalised allowing the subscript ℓ to run to several thousand if necessary.

The system we consider comprises two metal spheres separated by dielectric therefore both spheres must remain electrically neutral. This condition is automatically fulfilled for excitations with $m\neq 0$. For $m=0$ neutrality is ensured because the matrices $\mathbf{S}^{++},\mathbf{S}^{--}$ act as projection operators removing any charge transfer between the spheres. For example the matrices have respectively zero right eigenvectors,

$$
a^{0+}_{\ell'}=\frac{R_0^{-\ell'}}{\sqrt{2\ell'+1}}, \quad a^{0-}_{\ell'}=\frac{R_0^{\ell'}}{\sqrt{2\ell'+1}}. \tag{11}
$$

Orthogonality to these vectors ensures charge neutrality.

To demonstrate our methodology we apply our theory to calculating the modes of two identical spheres at various separations. We assume a plasmonic system characterised by a negative value of e'_M where $e'_M = -¥$ at zero frequency, $e'_M = 0$ at the bulk plasma frequency, typically in the UV/visible region of the spectrum, and $e'_M = -1$ at the surface plasma frequency. The Palik data for silver are used [26]. Omitting the imaginary part of e'_M is not essential to our calculations but gives a more critical test of our theory.

We choose spheres of radius $R'_1 = R'_2 = 5.0$ nm noting that in the quasi-static approximation systems are scale invariant. Choosing equal radii is not essential but simplifies interpretation as the modes factor into odd and even with respect to the symmetry plane. Fig. 2 shows our calculations for the modes at various separations of the spheres. Convergence was achieved including up to $\ell = 60$ partial waves and imposing the zero charge requirement. The tridiagonal nature of the matrices enabled the calculations to be done on a laptop at a rate of 0.002 seconds per eigenmode.

The results for the odd modes (closed circles) are easiest to understand: as the spheres approach the field distribution is pulled more and more into the gap greatly reducing the modes' frequencies because of the close proximity across the gap. Fig. 3a shows the spatial distribution of the modes both in the actual frame and in the transformed frame. Clearly the highly localised nature of the odd modes in real space would require many orders of spherical harmonics for an accurate description. In contrast in the transformed space the distributions are relatively smooth and required only a few spherical harmonics for an accurate description

In contrast the even modes fall into two categories: those which tend to the bulk plasma frequency as the gap is reduced, these we call the normal modes, and those which tend to another limit, these we call the anomalous modes. In contrast when two cylinders interact, there are no anomalous modes.

A plot of the field distribution shows what is happening. Just like the odd modes, the normal even modes, shown in Fig. 3b, are drawn into the gap where the repulsion of charges consequent on their even character drives up the frequency. In the transformed space these modes also have a relatively smooth distribution that is well described by a few spherical harmonics.

The anomalous modes, shown in Fig. 3c, appear to be modifications of the dipole, quadrapole, etcetera, modes of the isolated spheres. There is a 'bite' taken out of them from the gap region where the potential is almost

constant and the fields almost zero. Hence their frequencies are perturbed by only a small amount from those of the isolated sphere and this perturbation saturates as the spheres approach closely. Mapped into the transformed frame these fields show the opposite effect to the other modes: they are confined to the region near the origin and their most simple description is to be had in the original frame. These observations inspire us to seek an even simpler description of the fields. We ask the question if the fields can be described by assuming that the main part of the fields behaves like a single spherical harmonic but of fractional order. We then impose the requirement that the angular component of the field is zero at the origin and at some critical angle, θ_0, chosen empirically to fit the frequencies of the modes (as measured by the value of ϵ'_M at which they occur). This determines ν/n such that at infinite separation $\nu/n \to 1$,

$$dP_\nu/d\theta|_{\theta=0} = 0, \quad dP_\nu/d\theta|_{\theta=\theta_0} = 0, \tag{12}$$

where P_ν stands for the Legendre function of order ν. This condition also ensures that the modes have zero net charge on each sphere. Table 1 shows a comparison of the values of ϵ'_M (which imply the frequencies) at which the modes are found. Clearly our assumption of fractional ν makes an extremely good approximation to the anomalous modes.

In our work on cylinders [6] we have shown how to represent an incident plane wave in the original frame as a point dipole in the transformed frame. This enables us to calculate the absorption cross section for two nearly touching silver spheres which we show in Fig. 4 for the case that the incident electric field is aligned with the axis of the pair. In this case only the $m = 0$ modes are relevant.

Our quasi analytic calculations based on equation (6) are identical to simulations using the COMSOL codes but are computationally much more efficient by a factor of more than 10^3. Note that the cross section of the dimer is comparable to the physical cross section over a broad band of frequencies.

When two particles approach one another, quantum fluctuations in their charge density result in a force attracting the particles. At very large distances this force is extremely weak and is due to retarded dipole interactions between the fluctuations but as the particles approach the fluctuations become strongly correlated and the force greatly increases in magnitude. Also when all relevant distances are much smaller than a typical optical

wavelength retardation can be neglected and the quasi static approximation, which we assume in this article, is accurate. We can calculate the total energy of a system by integrating over the density of states weighted by the zero point energy,

$$\begin{aligned} U &= \frac{1}{2\pi i}\int_{-\infty}^{+\infty}\frac{1}{2}\hbar|\omega|\frac{\partial \ln\det \mathbf{D}}{\partial \omega}d\omega \\ &= \frac{\hbar}{2\pi i}\int_{0}^{+\infty}\mathrm{Im}\ln\det \mathbf{D}\, d\omega, \end{aligned} \tag{13}$$

where,

$$\mathbf{D}=\begin{bmatrix} 0 & \mathbf{T}^{+-} \\ \mathbf{T}^{+-} & 0 \end{bmatrix}^{-1}\begin{bmatrix} \mathbf{T}^{++} & \mathbf{T}^{+-} \\ \mathbf{T}^{-+} & \mathbf{T}^{--} \end{bmatrix}, \tag{14}$$

and hence the force by differentiating with respect to separation. In practice the integral is evaluated by rotating the contour to lie along the imaginary frequency axis where the integration is much easier to perform. A related approach using bispherical coordinates has been applied to a resistive, but not plasmonic, medium [27].

In addition to this calculation (exact within the quasi static approximation) we evaluate equation (13) approximating $\mathbf{T}$ by its diagonal elements in each of the four quadrants, but also imposing the charge neutrality condition as noted in equation (11). For the sphere-planar geometry his leads to the expression,

$$\begin{aligned} \ln\det \mathbf{D} &\approx \sum_{l=1}^{\infty}(2l+1)\ln(1-e^{2\alpha}\gamma^{2l+1}) \\ &+\ln\left[1-e^{2\alpha}\left(1-\gamma^{2}\right)\sum_{l=1}^{\infty}\frac{\gamma^{2l+1}}{1-e^{2\alpha}\gamma^{2l+1}}\left(1-\gamma^{2l}\right)\right] \end{aligned} \tag{15}$$

where $\gamma = R_1/R_2$. Fig. 5 shows the results of these calculations assuming a plasmonic form for the metal permittivity,

$$\varepsilon = 1-\frac{\omega_p^2}{\omega(\omega+i\gamma)}, \tag{16}$$

where $\gamma/\omega_p = 0.05$. It is evident that, although approximate, equation (15) gives a very accurate value for the force. We also show the well known proximity force approximation (PFA) [28] which is accurate for extremely small separations but clearly fails for more modest separations where our formula works well.

In this article we have presented a new approach to calculating the properties of singular 3D objects, in our example two spheres, based on transformation optics. We have demonstrated its computational effectiveness in evaluating the modal frequencies, the system's response to incoming radiation, and the Van der Waals forces acting between the spheres. In addition our method lends itself to accurate approximations which both elucidate the physical nature of processes at work and show the way forward to computations that would otherwise be extremely time consuming.

Acknowledgements

For our support we thank the following: AIFD and JBP the Gordon and Betty Moore Foundation, JBP the AFOSR, RZ the Royal Commission for the Exhibition of 1851, YL and JBP the Leverhulme Trust.

References

[1] Ward, A. J. and Pendry, J. B., Refraction and geometry in Maxwell's equations. *Journal of Modern Optics* **43** 773-93 (1996).

[2] Shyroki, D.M., Note on transformation to general curvilinear coordinates for Maxwell's curl equations. *http://arxiv.org/abs/physics/0307029v1* (2003)

[3] Schurig, D., Pendry, J. B., Smith, D.R., Calculation of material properties and ray tracing in transformation media. *Optics Express*, **14**, Issue 21, 9794-9804 (2006).

[4] Leonhardt, U., "Transformation optics and the geometry of light. *Prog. Opt.*, **53**, 70-152 (2009).

[5] Kundtz, N. B., Smith, D. R., J. B. Pendry, Electromagnetic design with transformation optics. *Proc. IEEE*, **99**, 1622-3 (2011).

[6] Pendry, J. B., Aubry, A., Smith, D. R., Maier, S. A., Transformation optics and subwavelength control of light. *Science* **337,** 549-52 (2012).

[7] Pendry, J. B., Perfect Cylindrical lenses. *Opt. Exp.*, **11**, 755–760, (2003).

[8] Pendry, J. B., Negative refraction makes a perfect lens. *Phys. Rev. Lett.*,**85**, 3966-9 (2000).

[9] Leonhardt, Optical Conformal Mapping. U., *Science*, **312** 1777–1780, (2006).

[10] Pendry, J. B., Schurig, D., and Smith, D.R., Controlling electromagnetic fields. *Science* **312** 1780-2 (2006).

[11] McPhedran, R. C., and McKenzie, D. R., Electrostatic and optical resonances of arrays of cylinders. *Appl. Phys. A*, **23** 223–235, (1980).

[12] McPhedran, R. C., and Perrins, W. T., Electrostatic and optical resonances of cylinder pairs. *Appl. Phys. A*, **24** 311–318, (1981).

[13] McPhedran, R. C., and Milton, G. W., Transport properties of touching cylinder pairs and of the square array of touching cylinders. *Proc. R. Soc. A*, **411** 313–326, (1987).

[14] Garc á Vidal, F.J. and Pendry, J. B., A collective theory for surface enhanced Raman scattering. *Phys. Rev. Lett.*, **77** 1163–1166, (1996).

[15] Stockman, M.I., Nanofocusing of optical energy in tapered plasmonic waveguides. *Phys. Rev. Lett.*, **93** 137404, (2004).

[16] Talley, C. E., Jackson, J. B., Oubre, C., Grady, N. K., Hollars, C. W., Lane, S. M., Huser, T. R., and Nordlander, P., Surface-enhanced Raman scattering from individual Au nanoparticles and nanoparticle dimer substrates. *Nano Lett.*, **5** 1569–1574, (2005).

[17] Sweatlock, L.A., Maier, S.A., Atwater, H.A., Penninkhof, J.J., and Polman, A., Highly confined electromagnetic fields in arrays of strongly coupled Ag nanoparticles. *Phys. Rev. B*, **71** 235408, (2005).

[18] Romero, I., Aizpurua, J., Bryant, G.W., and Garcıa de Abajo, F.J., Plasmons in nearly touching metallic nanoparticles: singular response in the limit of touching dimers. *Opt. Exp.*, **14** 9988–9999, (2006).

[19] Hill, R. T., Mock, J. J., Urzhumov, Y., Sebba, D. S., Oldenburg, S. J., Chen, S.Y., Lazarides, A. A., Chilkoti, A., and Smith, D.R., Leveraging nanoscale plasmonic modes to achieve reproducible enhancement of light. *Nano Lett.*, **10** 4150–4154, (2010).

[20] Schuller, J. A., et al., Plasmonics for extreme light concentration and manipulation. *Nat. Mater*. **9**, 193 (2010).

[21] Nordlander, P., Oubre, C., Prodan, E., Li, K., and Stockman, M. I., Plasmon hybridization in nanoparticle dimers. *Nano Lett.*,**4** 899–903, (2004).

[22] Garc á de Abajo, F.J. , Nonlocal effects in the plasmons of strongly interacting nanoparticles, dimers, and waveguides. *J. Phys. Chem. C*, **112**,17983–17987, (2008).

[23] Aizpurua, J. and Rivacoba, S., *Phys. Rev.* Nonlocal effects in the plasmons of nanowires and nanocavities excited by fast electron beams. B78, 035404 (2008).

[24] Esteban, R., Borisov, A. G., Nordlander, P., and Aizpurua, J., Bridging quantum and classical plasmonics with a quantum-corrected model. *Nat. Commun.* **3**, 825 (2012).

[25] Savage, K.J., Hawkeye, M.M., Esteban, R., Borisov, A. G., Aizpurua, J., and Baumberg, J. J., Revealing the quantum regime in tunnelling plasmonics. *Nature*, **491**, 574–577 (2012).

[26] Palik, E. D., *Handbook of Optical Constants of Solids*, Academic Press, New York (1985).

[27] Bimonte, G., and Emig, T., Exact results for classical Casimir interactions: Dirichlet and Drude model in the sphere-sphere and sphere-plane geometry. *Phys. Rev. Lett.***109**, 160403 (2012).

[28] Israelachvili, J.N., *Intermolecular and Surface Forces*, Academic Press Inc., San Diego (1998).

Table

	zero gap		gap = 3.5 nm	
n	$n = \sqrt{2}n$	exact	$n = 1.225n$	exact
1	-1.7071	-1.6962	-1.8163	-1.7844
2	-1.3536	-1.3557	-1.4082	-1.4079
3	-1.2357	-1.2421	-1.2721	-1.2810
4	-1.1768	-1.1838	-1.2041	-1.2170
5	-1.1414	-1.1474	-1.1633	-1.1787

Table 1.Values of ε'_M (which determine the frequencies of the modes) for the anomalous even modes of two spheres each of diameter10 nm, calculated assuming a fractional value n of n for the Legendre function in real space.

Figure captions

Figure 1 a) the starting structure consists of a dielectric annulus defined by a sphere and a hollow sphere. b) performing an inversion about a point within the annulus gives rise to two spheres of radii and separation defined by the annular system and the point of inversion. Coordinates for Fig. 1b are primed to distinguish from the annulus.

Figure 2 Modes of two 5 nm radius spheres for various separations a) for $m = 0$ and b) $m = 5$. The even modes are represented by open circles, the odd by closed circles. As the gap narrows the odd modes tend to zero frequency, $e'_M(w = 0) = -¥$, and some of the even modes tend to the bulk plasma frequency, $e'_M(w = w_p) = 0$. However there is another set of even modes that tend to other intermediate limits.

Figure 3 The potential distribution shown in real space and in the transformed space for two spheres each 10 nm in diameter, separated by 0.4 nm.The mode order increases left to right from unity to three. For all figures $m = 0$ as in panel a) of Fig. 2. a) the odd modes at 3.536, 3.582, and 3.597 eV; b) the normal even modes at 3.703, 3.673, and 3.652 eV; c) the anomalous even modes at 3.028, 3.418 and 3.523 eV. Blue denotes the minimum potential, red the maximum, and green zero potential.

Figure 4 The absorption cross section for 10 nm diameter silver spheres separated by 0.1 nm compare to the physical cross section. Our quasi analytic theory is compared to simulations. The permittivity of silver was taken from Palik's data [26].

Figure 5 The Van der Waals force acting between a small metallic sphere and a metallic surface as a function of distance. The permittivity given in eq. (16) describes a plasmonic system. a) the fully converged exact force in units of $\hbar w_p / R$. b) deviation from the exact force of the proximity force approximation (PFA), dashed line, and our approximate formula, full line.

Figures

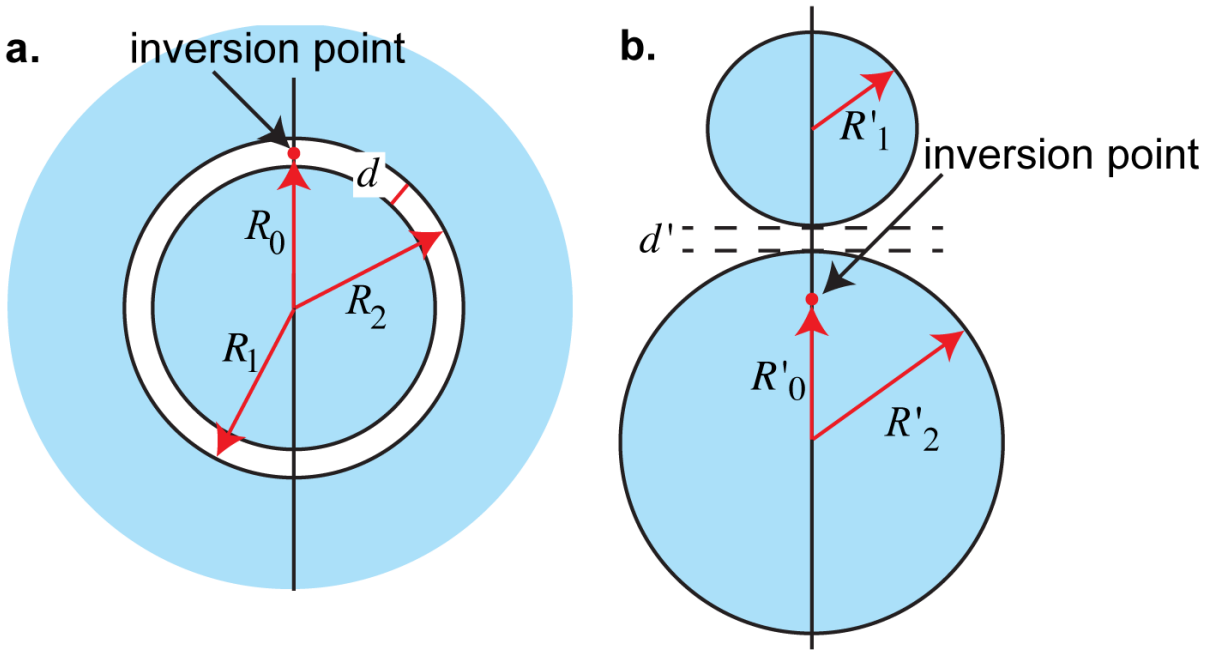

Figure 1 a) the starting structure consists of a dielectric annulus defined by a sphere and a hollow sphere. b) performing an inversion about a point within the annulus gives rise to two spheres of radii and separation defined by the annular system and the point of inversion. Coordinates for Fig. 1b are primed to distinguish from the annulus.

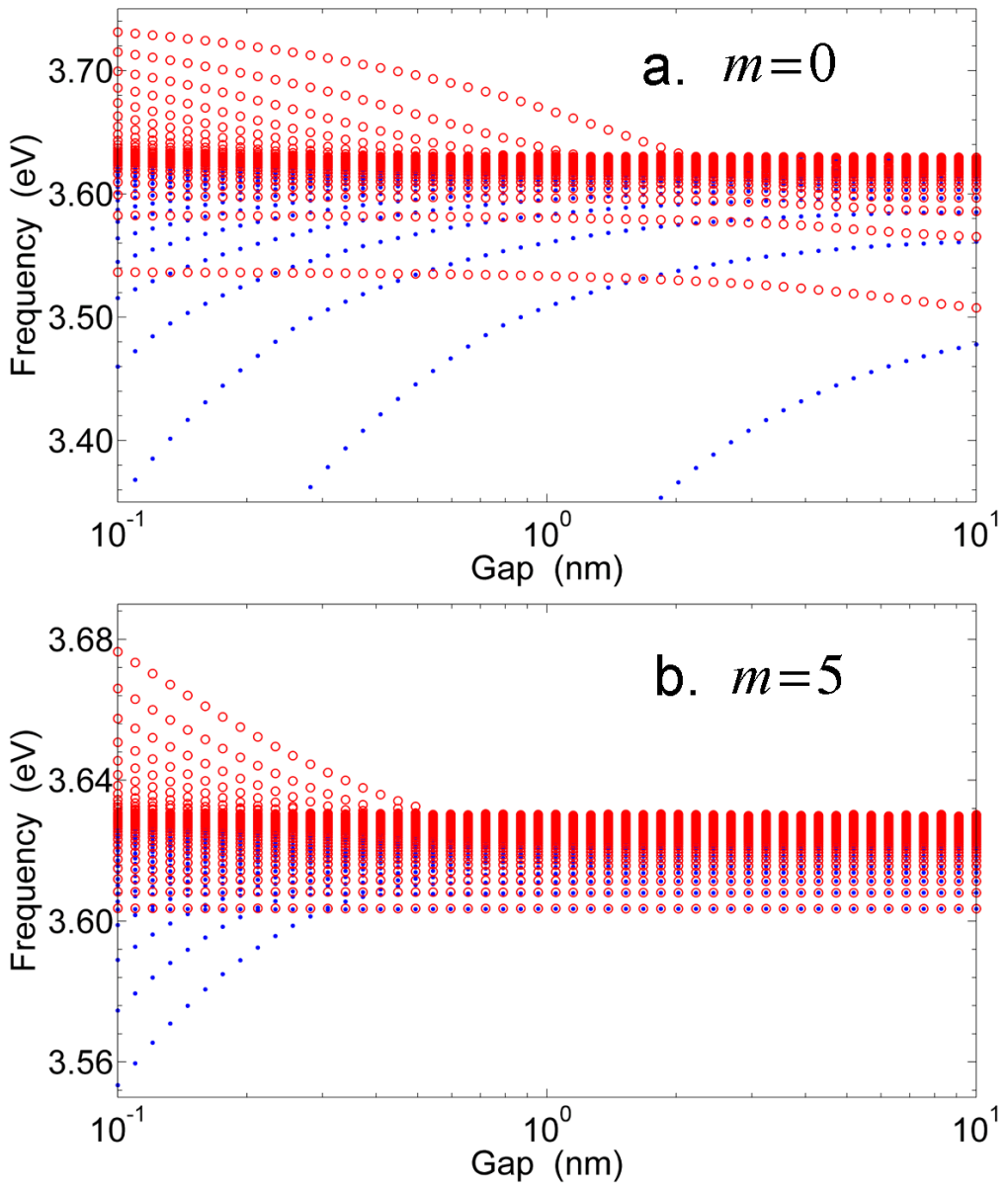

Figure 2 Modes of two 5 nm radius spheres for various separations a) for $m=0$ and b) $m=5$. The even modes are represented by open circles, the odd by closed circles. As the gap narrows the odd modes tend to zero frequency, $e'_M(w=0)=-¥$, and some of the even modes tend to the bulk plasma frequency, $e'_M\left(w=w_p\right)=0$. However there is another set of even modes that tend to other intermediate limits.

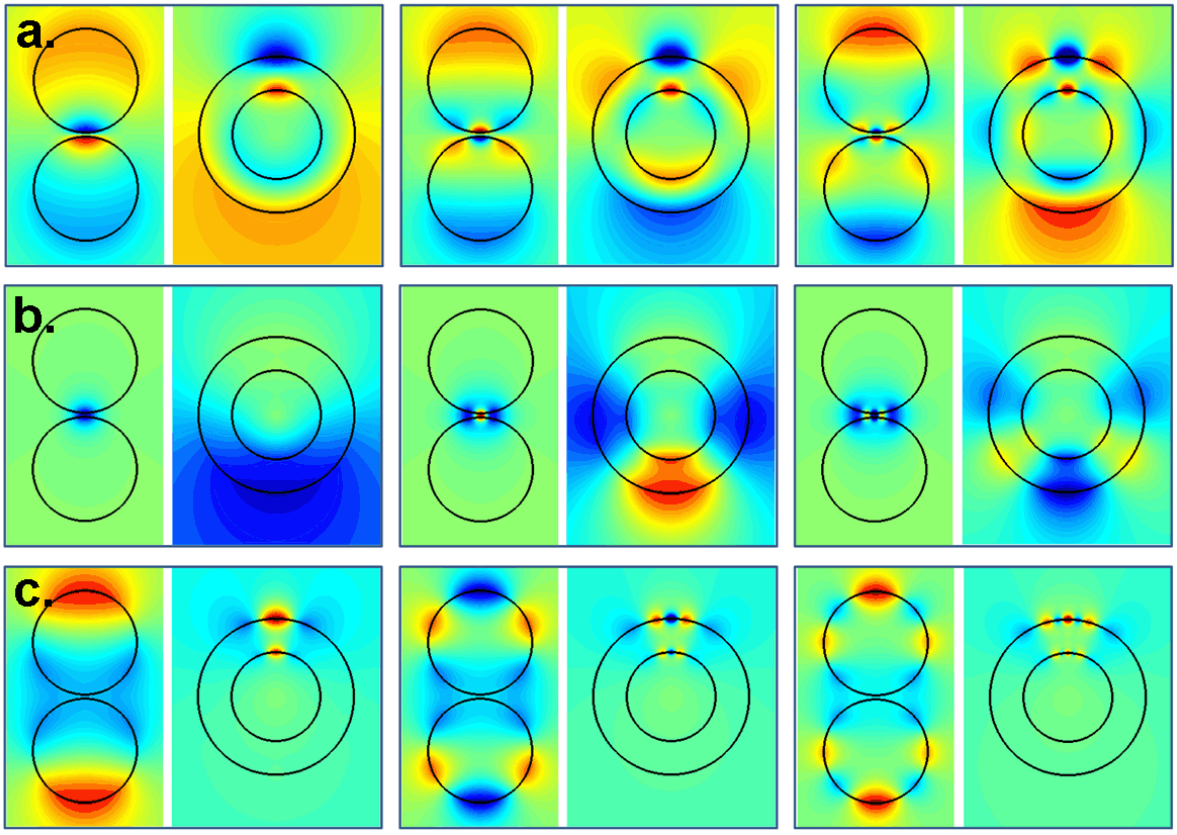

Figure 3 The potential distribution shown in real space and in the transformed space for two spheres each 10 nm in diameter, separated by 0.4 nm. The mode order increases left to right from unity to three. For all figures $m = 0$ as in panel a) of Fig. 2.

a) the odd modes at 3.536, 3.582, and 3.597 eV; b) the normal even modes at 3.703, 3.673, and 3.652 eV; c) the anomalous even modes at 3.028, 3.418 and 3.523 eV. Blue denotes the minimum potential, red the maximum, and green zero potential.

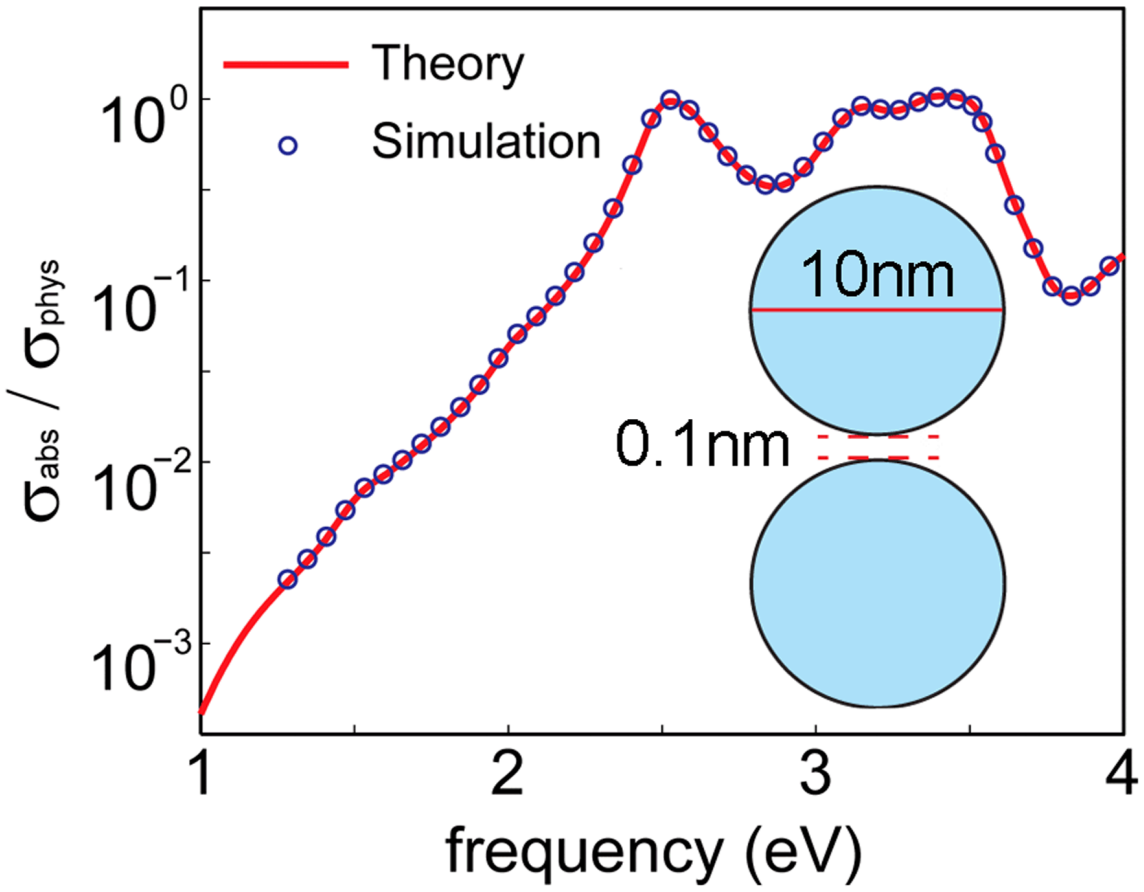

Figure 4 The absorption cross section for 10 nm diameter silver spheres separated by 0.1 nm compare to the physical cross section. Our quasi analytic theory is compared to simulations. The permittivity of silver was taken from Palik's data [26].

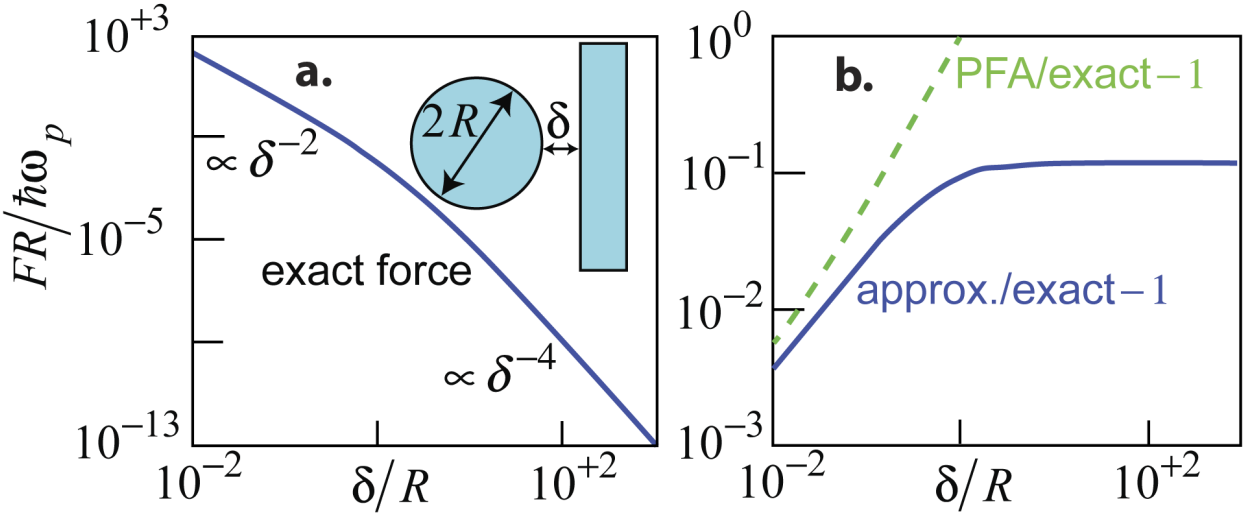

Figure 5 The Van der Waals force acting between a small metallic sphere and a metallic surface as a function of distance. The permittivity given in eq. (16) describes a plasmonic system. a) the fully converged exact force in units of $\hbar w_p/R$. b) deviation from the exact force of the proximity force approximation (PFA), dashed line, and our approximate formula, full line.